J|A|C|S
ARTICLES

Published on Web 11/26/2008

Fully Conjugated Tri(perylene bisimides): An Approach to the Construction of *n*-Type Graphene Nanoribbons

Hualei Qian,[†,§] Fabrizia Negri,[*,‡] Chunru Wang,[†] and Zhaohui Wang[*,†]

Beijing National Laboratory for Molecular Sciences, Institute of Chemistry, Chinese Academy of Sciences, Beijing 100190, China, Dipartimento di Chimica "G. Ciamician", Unversità di Bologna, Via F. Selmi 2, 40126 Bologna, Italy and INSTM, UdR Bologna, Italy, and Graduate School of the Chinese Academy of Sciences, Beijing 100190, China

Received October 2, 2008; E-mail: fabrizia.negri@unibo.it; wangzhaohui@iccas.ac.cn

Abstract: We present an experimental study encompassing synthesis and characterization of fully conjugated tri(perylene bisimides) (triPBIs), having 19 six-membered carbon rings in the core and six imide groups at the edges. Two structural isomers of triPBIs resulting from the two probable coupling positions were successfully separated by HPLC. To assist the identification of the two structural isomers, quantum-chemical calculations of electronic structure, NMR, and optical spectra were carried out. Calculations predict stable helical and nonhelical configurations for both triPBIs isomers and allow the assignment of triPBIs **6** unequivocally to the most bathochromically shifted absorption spectrum. Increasing the number of PBI units in oligo-PBIs leads to an expansion of the π system, in turn associated with a reduction of the transport and optical band gaps, and a remarkable increase in electron affinities, which make oligo-PBIs promising n-type functional components in optoelectronic devices.

Introduction

Graphene nanoribbons (GNRs), for which the width of the sheet is confined to be a finite size while the length is considered infinitely long, have attracted considerable interest due to their high potential for technological applications, mostly in GNRs-based nanoelectronics.[1] Driven by these, a great effort has been devoted to developing methods for preparation of GNRs. Lithographic patterning of graphene sheets has led to the fabrication of GNRs down to widths of ~20 nm thus far,[2] but there are difficulties in obtaining smooth edges and reaching true nanometer-scale ribbon width. Quite recently, Dai developed a chemical method for making 10 nm wide GNRs just one atom thick and demonstrated their promising semiconducting properties for electronic applications.[3] Müllen also reported a new synthetic protocol yielding linear GNRs with length up to 12 nm which was never achieved before.[4] As GNRs consist of infinite repeating polycyclic aromatic units in one dimension, which can be easily decorated, bottom-up organic synthetic methodologies can be regarded as the most promising routes to functionalized graphene nanoribbons (F-GNRs).

Molecular systems based on perylene bisimides **1** (PBIs) have been extensively investigated in recent years, primarily due to their industrial applications as dyes and pigments.[5] Moreover, their versatile optical and electrochemical properties,[6] the possibility to tune these properties by grafting various substituents at their bay positions,[7] their high electron affinity,[8] and their chemical and thermal stabilities make PBIs attractive n-type materials in electronics and optoelectronics.[9] In these respects, core-expanded PBIs such as coronene, terrylene, and quaterrylene bisimides have been demonstrated to have important uses for liquid-crystal materials, single-molecule spectroscopy, and near-infrared-absorbing dyes.[10] Since the imide groups have a great influence on properties and applications of PBIs, it is interesting to modify GNRs with arrays of electron-withdrawing imide groups. Accordingly, we attempted to construct F-GNRs by repeating the PBI unit in one dimension, that is, designing

[†] Institute of Chemistry, Chinese Academy of Sciences.
[§] Graduate School of the Chinese Academy of Sciences.
[‡] Unversità di Bologna and INSTM.

(1) (a) Novoselov, K. S.; Geim, A. K.; Morozov, S. V.; Jiang, D.; Zhang, Y.; Dubonos, S. V.; Grigorieva, I. V.; Firsov, A. A. *Science* **2004**, *306*, 666–669. (b) Geim, A. K.; Novoselov, K. S. *Nat. Mater.* **2007**, *6*, 183–191. (c) Watson, M. D.; Fechtenkötter, A.; Müllen, K. *Chem. Rev.* **2001**, *101*, 1267–1300. (d) Tsefrikas, V. M.; Scott, L. T. *Chem. Rev.* **2006**, *106*, 4868–4884.
(2) Han, M. Y.; Özyilmaz, B.; Zhang, Y.; Kim, P. *Phys. Rev. Lett.* **2007**, *98*, 206805.
(3) (a) Li, X.; Wang, X.; Zhang, L.; Lee, S.; Dai, H. *Science* **2008**, *319*, 1229–1232. (b) Wang, X.; Ouyang, Y.; Li, X.; Wang, H.; Guo, J.; Dai, H. *Phys. Rev. Lett.* **2008**, *100*, 206803.
(4) Yang, X.; Dou, X.; Rouhanipour, A.; Zhi, L.; Rader, H. J.; Müllen, K. *J. Am. Chem. Soc.* **2008**, *130*, 4216–4217.
(5) (a) Herbst, W.; Hunger, K. *Industrial Organic Pigments: Production, Properties, Applications* , 2nd ed.; Wiley-VCH: Weinheim, 1997. (b) Zollinger, H. *Color Chemistry*, 3rd ed.; VCH: Weinheim, 2003.
(6) (a) Würthner, F. *Chem.Commun.* **2004**, 1564–1579. (b) Wasielewski, M. R. *J. Org. Chem.* **2006**, *71*, 5051–5066.
(7) (a) Zhao, Y.; Wasielewski, M. R. *Tetrahedron Lett.* **1999**, *40*, 7047–7050. (b) Rohr, U.; Kohl, C.; Müllen, K.; van de Craats, A.; Warman, J. *J. Mater. Chem.* **2001**, *11*, 1789–1799. (c) Würthner, F.; Sautter, A.; Schilling, J. *J. Org. Chem.* **2002**, *67*, 3037–3044. (d) Serin, J. M.; Brousmiche, D. W.; Frechet, J. M. J. *J. Am. Chem. Soc.* **2002**, *124*, 11848–11849. (e) Chen, Z.; Debije, M. G.; Debaerdemaeker, T.; Osswald, P.; Würthner, F. *ChemPhysChem* **2004**, *5*, 137–140. (f) Chao, C.; Leung, M.; Su, Y. O.; Chiu, K.; Lin, T.; Shieh, S.; Lin, S. *J. Org. Chem.* **2005**, *70*, 4323–4331. (g) Osswald, P.; Leusser, D.; Stalke, D.; Würthner, F. *Angew. Chem., Int. Ed.* **2005**, *44*, 250–253. (h) Qian, H.; Liu, C.; Wang, Z.; Zhu, D. *Chem. Commun.* **2006**, 4587–4589. (i) Würthner, F.; Osswald, P.; Schmidt, R.; Kaiser, T. E.; Mansikkamäki, H.; Könemann, M. *Org. Lett.* **2006**, *8*, 3765–3768. (j) Li, Y.; Wang, Z.; Qian, H.; Shi, Y.; Hu, W. *Org. Lett.* **2008**, *10*, 529–532.
(8) Lee, S. K.; Zu, Y.; Herrmann, A.; Geerts, Y.; Müllen, K.; Bard, A. J. *J. Am. Chem. Soc.* **1999**, *121*, 3513–3520.

 10.1021/ja807803j CCC: $40.75

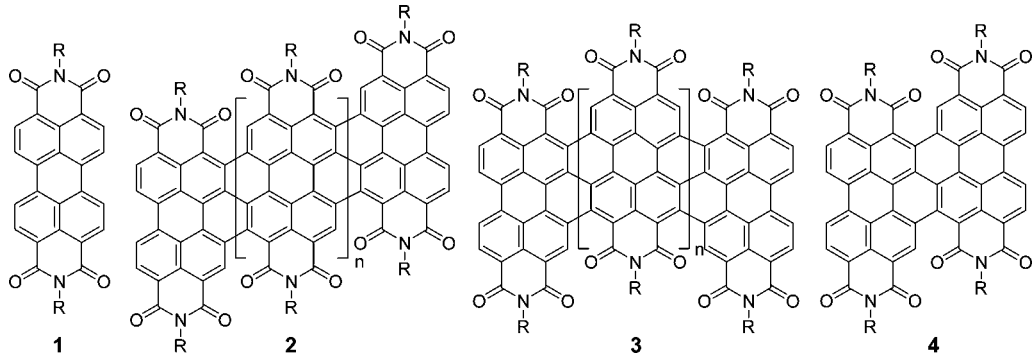

Figure 1. PBIs **1**, poly(PBIs) **2** and **3**, and diPBIs **4**.

poly(PBIs) **2** or **3** (poly(PBIs) having several probable isomeric structures, two of which are shown in Figure 1).

As shown in other studies,[11] π-conjugated oligomers with precisely defined length and constitution are regarded as ideal model compounds for elucidating properties of high-molecular-weight polymers. In the course of our research on oligomeric or polymeric PBIs, we have prepared triply linked di(perylene bisimides) **4** (diPBIs) by copper-mediated coupling of tetrachloro-PBIs,[12] the aromatic cores of which are enlarged more than twice along the bay positions. Herein we present an experimental study encompassing synthesis and characterization of fully conjugated tri(perylene bisimides) **5** and **6** (triPBIs), which have 19 six-membered carbon rings in the core and 6 imide groups at the edges. The structures of triPBIs **5** and **6** are determined by ^{1}H NMR and MALDI-TOF spectroscopy. Due to differences in the molecular structures and the degree of π electron delocalization, two isomers of triPBIs **5** and **6** exhibit different optical and electrochemical properties, providing an ideal model for a systematic study of structure−property relationships of GNRs. To assist the identification of the two structural isomers of triPBIs, quantum-chemical calculations of electronic structure, NMR spectra, and optical spectra are carried out. Furthermore, computations are employed to investigate the evolution of structures and properties from PBIs to diPBIs to triPBIs, which are useful for predicting specific information on photonic and electronic properties of the corresponding higher oligomeric or polymeric analogues.

Computational Details

Atomic structures of **1**, **4**, **5**, and **6** were optimized with density functional theory (DFT) calculations using the B3LYP hybrid functional[13] with the basis set limited to 3-21G owing to the large dimension of the chromophores. Molecular orbital shapes and energies discussed in the text are those calculated at the optimized geometries. Orbital pictures were prepared with Molekel 4.3 visual software.[14]

Chemical shifts were calculated with the gauge-including atomic orbitals (GIAO) theory[15] and were plotted with Gaussview[16] using as reference the B3LYP/3-21G results for TMS. Electronic excitation energies and oscillation strengths were computed for the 60 lowest singlet excited electronic states of **4**, **5**, and **6** with time-dependent (TD) DFT calculations. In plotting computed electronic spectra, a Lorentzian line width of 0.1 eV was superimposed to each computed intensity to facilitate comparison with experimental spectra. All quantum-chemical calculations were performed with the Gaussian03 package.[17]

Synthesis and Characterization

As revealed by the synthesis of diPBIs **4**,[12] only two chlorine substituents in one bay region of PBIs can participate in copper-mediated coupling reaction, probably because of the low reactivity of chlorides. The reactivity of the precursor as well as the reaction temperatures are presumed to be key factors to expand the PBI unit along the two bay regions. Accordingly, we used tetrabromo-PBI instead of chloride as the precursor and conducted the coupling reaction at 110 °C under the system of CuI, L-proline, and K_2CO_3 (Scheme 1). According to the MALDI-TOF spectroscopy, diPBI, triPBIs, and tetraPBIs were observed in the products of the coupling reaction. After purification on silica column chromatography, triPBIs were obtained as dark-green solids in 16%, which indicates that simultaneous coupling in both bay regions of

(9) (a) Ranke, P.; Bleyl, I.; Simmerer, J.; Haarer, D. *Appl. Phys. Lett.* **1997**, *71*, 1332–1334. (b) Dittmer, J. J.; Marseglia, E. A.; Friend, R. H. *Adv. Mater.* **2000**, *12*, 1270–1274. (c) Schmidt-Mende, L.; Fechtenkötter, A.; Müllen, K.; Moons, E.; Friend, R. H.; Mackenzie, J. D. *Science* **2001**, *293*, 1119–1122. (d) Ego, C.; Marsitzky, D.; Becker, S.; Zhang, J.; Grimsdale, A. C.; Müllen, K.; Mackenzie, J. D.; Silva, C.; Friend, R. H. *J. Am. Chem. Soc.* **2003**, *125*, 437–443. (e) Jones, B. A.; Ahrens, M. J.; Yoon, M.; Facchetti, A.; Marks, T. J.; Wasielewski, M. R. *Angew. Chem., Int. Ed.* **2004**, *43*, 6363–6366. (f) Shin, W. S.; Jeong, H.; Kim, M.; Jin, S.; Kim, M.; Lee, J.; Lee, J. W.; Gal, Y. *J. Mater. Chem.* **2006**, *16*, 384–390. (g) Jones, B. A.; Facchetti, A.; Wasielewski, M. R.; Marks, T. J. *J. Am. Chem. Soc.* **2007**, *129*, 15259–15278. (h) Brédas, J. L.; Beljonne, D.; Coropceanu, V.; Cornil, J. *Chem. Rev.* **2004**, *104*, 4971–5004. (i) Coropceanu, V.; Cornil, J.; da Silva, D. A.; Olivier, Y.; Silbey, R.; Brédas, J. L. *Chem. Rev.* **2007**, *107*, 926–952. (j) Cornil, J.; Beljonne, D.; Carlbert, J. P.; Brédas, J. L. *Adv. Mater.* **2001**, *13*, 1053–1067.

(10) (a) Holtrup, F.; Müller, G.; Quante, H.; Feyter, S.; Schryver, F. C.; Müllen, K. *Chem. Eur. J.* **1997**, *3*, 219–225. (b) Geerts, Y.; Quante, H.; Platz, H.; Mahrt, R.; Hopmeier, M.; Böhm, A.; Müllen, K. *J. Mater. Chem.* **1998**, *8*, 2357–2369. (c) Rohr, U.; Schlichting, P.; Böhm, A.; Gross, M.; Meerholz, K.; Bräuchle, C.; Müllen, K. *Angew. Chem., Int. Ed.* **1998**, *37*, 1434–1437. (d) Cotlet, M.; Vosch, T.; Habuchi, S.; Well, T.; Müllen, K.; Hofkens, J.; Schryver, F. *J. Am. Chem. Soc.* **2005**, *127*, 9760–9768.

(11) (a) Tour, J. M. *Chem. Rev.* **1996**, *96*, 537–553. (b) Martin, R. E.; Diederich, F. *Angew. Chem., Int. Ed.* **1999**, *38*, 1350–1377. (c) Nelson, J. C.; Saven, J. G.; Moore, J. S.; Wolynes, P. G. *Science* **1997**, *277*, 1793–1796. (d) Tsuda, A.; Osuka, A. *Science* **2001**, *293*, 79–82.

(12) (a) Qian, H.; Wang, Z.; Yue, W.; Zhu, D. *J. Am. Chem. Soc.* **2007**, *129*, 10664–10665. (b) Shi, Y.; Qian, H.; Li, Y.; Wang, Z. *Org. Lett.* **2008**, *10*, 2337–2340.

(13) (a) Becke, A. D. *Phys. Rev. A* **1988**, *38*, 3098–3100. (b) Lee, C.; Yang, W.; Parr, G. G. *Phys. Rev. B* **1988**, *37*, 785–789.

(14) Flükiger, P.; Lüthi, H. P.; Portman, S.; Weber, J. *Molekel*, version 4.3; Swiss National Supercomputing Centre CSCS: Manno, Switzerland, 2000 (http://www.cscs.ch/molekel/). Portmann, S.; Lüthi, H. P. *Chimia* **2000**, *54*, 766.

(15) (a) Ditchfield, R. *J. Chem. Phys.* **1972**, *56*, 5688–5691. (b) Wolinski, K.; Hinton, J. F.; Pulay, P. *J. Am. Chem. Soc.* **1990**, *112*, 8251–8260.

(16) Dennington, R., II; Keith, T.; Millam, J.; Eppinnett, K.; Hovell, W. L.; Gilliland, R. *GaussView*, Version 3.09; Semichem, Inc.: Shawnee Mission, KS, 2003.

(17) Frisch, M. J.; et al. *Gaussian 03*, revision C.02; Gaussian, Inc.: Pittsburgh, PA, 2003.

Scheme 1. Synthesis of triPBIs **5** and **6**

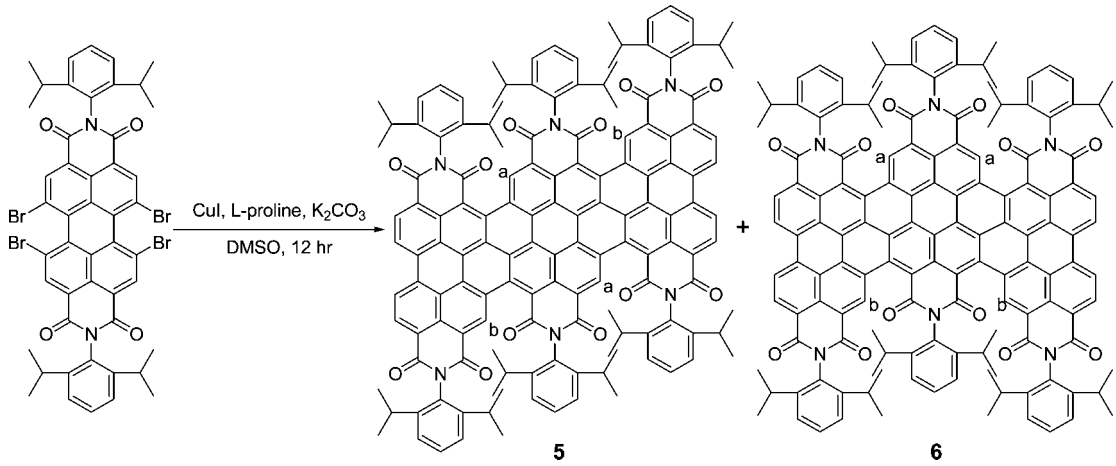

PBI is achieved, and therefore opens the door to higher oligomeric and polymeric PBIs. Notably, for the central PBI unit, the participant C−H bonds can be in different or the same naphthalene rings, the two possibilities resulting in two isomeric structures of triPBIs **5** and **6**. Using toluene as the eluent, triPBIs were successfully separated by HPLC to two fractions with peaks at 17 and 23 min, namely the first and second fraction (Figure 2), MALDI-TOF spectroscopy of which displayed the parent-ion peaks at $m/z = 2118.1$ and 2118.2, respectively (calcd for triPBI ($C_{144}H_{114}N_6O_{12}$), 2118.8 $[M]^-$). The structure of tri(perylene bisimides) was verified by the well-resolved ^1H and ^{13}C NMR spectroscopy obtained from the second fraction. The ^1H spectrum of the second fraction recorded in *o*-$C_6D_4Cl_2$ at 383 K (Figure 3) shows the characteristic signals at 2.81 (6H) and 3.11 ppm (6H) for 12 protons of isopropyl groups, and two sets of singlet peaks at 10.44 (2H) and 10.57 ppm (2H), respectively, for the aromatic protons neighboring oxygen atoms.

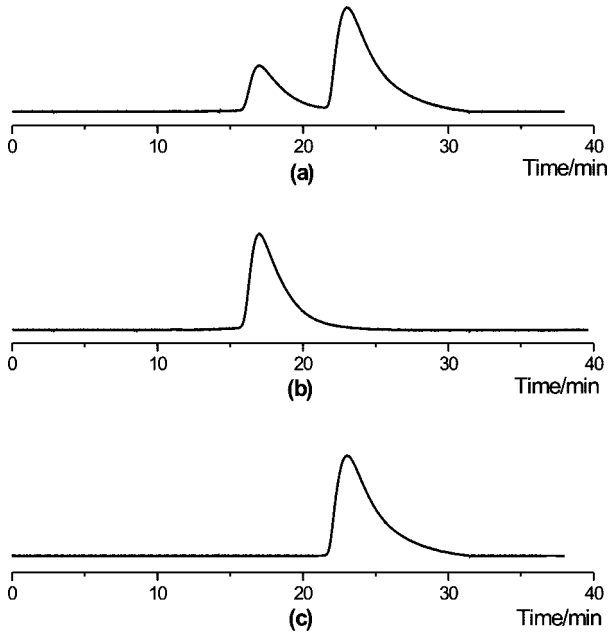

Figure 2. HPLC (Buckyprep column, toluene eluent at 12 mL/min) chromatograms: (a) triPBIs before separation, (b) the first fraction after separation, and (c) the second fraction after separation.

As can be seen from the ^1H spectra of the first and second fractions recorded in $CDCl_3$ at room temperature (Figure 4),[18] the NMR signals that mark the difference between the two structural isomers are those due to H_a and H_b. The chemical shift of these protons is considerably different for the first fraction and is rather similar for the second fraction.

Helical and Nonhelical Structures of F-GNRs. To investigate the structural changes of imide group functionalized GNRs occurring upon increasing the number of PBI units, and to assist the assignment of the NMR spectra of the two triPBI isomers, quantum chemical calculations were carried out on models for PBI **1**, diPBI **4**, and triPBIs **5** and **6**, featuring methyl substituents instead of isopropyl units on the phenyl rings. The computed structures of **1** and **4** (Figure S5 and S6, Supporting Information) indicate that the addition of one PBI unit leads to an out-of-plane twisting of the aromatic core,[19] driven by the steric congestion between oxygen and the neighboring hydrogen atom.

A similar trend, namely a considerable twisting of each PBI unit with respect to the others, is computed also for triPBIs whose equilibrium structures are distorted out of plane for both isomeric forms **5** (Figure 5) and **6** (Figure 6). More precisely, two low-energy conformers were optimized for both **5** and **6**, representing two different out-of plane deformations of the three PBI moieties. In both isomers, each PBI unit is twisted with respect to the adjacent one, similar to the observation with **4**. However, for three PBI units there are two pairs of adjacent PBI units, and one obtains two different out-of-plane conformational isomers. In one isomer, the two pairs of adjacent PBI units bend in the same direction so as to form a helical structure (with two enantiomeric forms), while in the second isomer the two pairs of adjacent PBI units bend in opposite directions, resulting in a nonhelical structure (a meso-configuration). Notably, for both **5** and **6**, the difference in absorption spectra (and molecular orbital energies) between the helical and nonhelical structures is almost negligible. From the above discussion it can be inferred that F-GNRs $(PBI)_n$ will be characterized by having as many as $n - 1$ possible out-of-plane

(18) Notably, the dramatic difference in appearance between the NMR spectra in Figures 3 and 4 is probably due to the solvent effect and aggregations that are not uncommon for large PAHs.

(19) (a) Osswald, P.; Würthner, F. *J. Am. Chem. Soc.* **2007**, *129*, 14319–14326. (b) Würthner, F. *Pure Appl. Chem.* **2006**, *78*, 2341–2349.

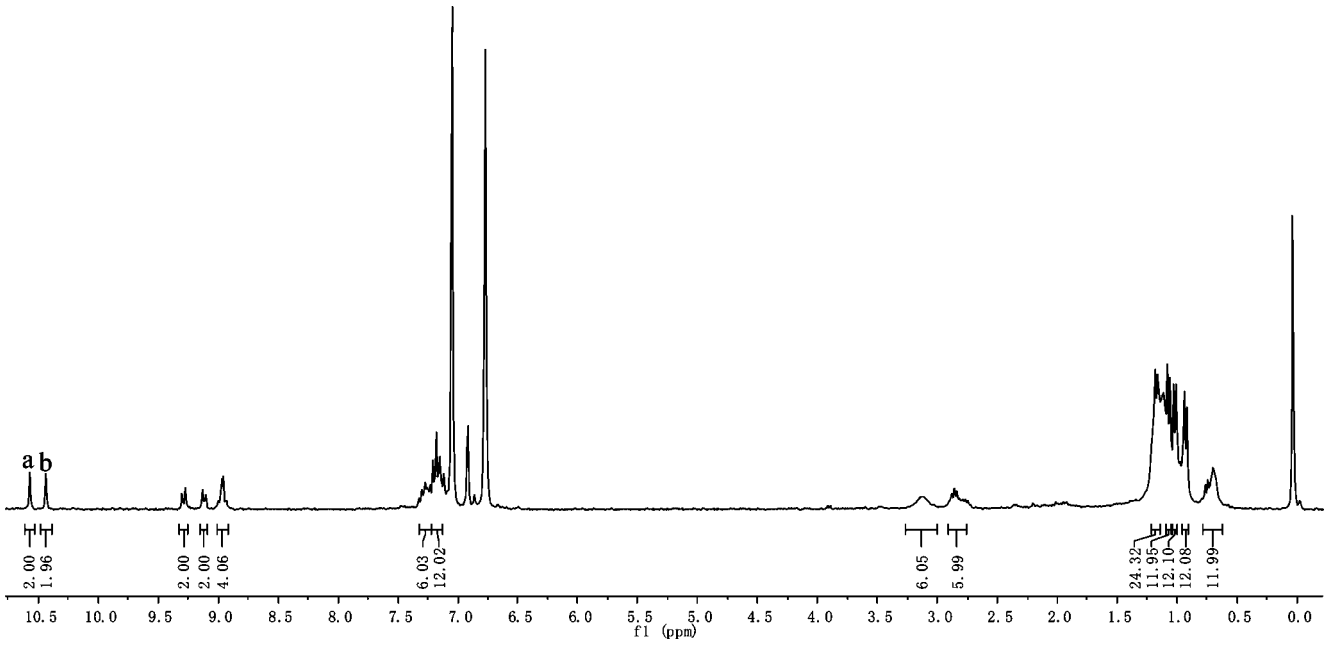

Figure 3. ^{1}H spectrum of the second fraction recorded in *o*-$C_6D_4Cl_2$ at 383 K.

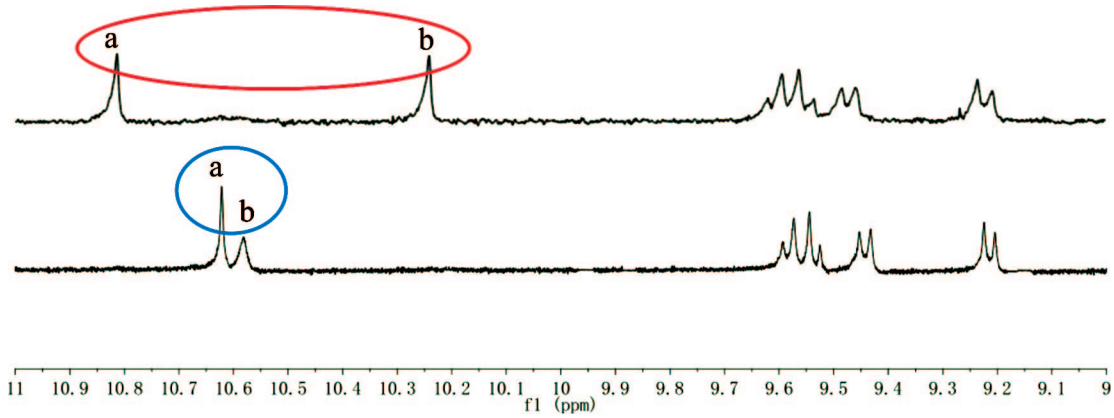

Figure 4. Selected part of the ^{1}H spectra of the first (top) and second (bottom) fractions recorded in $CDCl_3$ at room temperature.

structures of similar energy, of which one is helical (all the PBI pairs twisted in the same direction) and the remainder are nonhelical.

The NMR spectra were computed for the helical and nonhelical structures of **5** and **6**. The portions of the computed NMR spectra pertinent to H_a and H_b are shown in Figure 7. The spectra computed for the two isomers (helical and nonhelical) of **5** show similar chemical shift differences for H_a and H_b. Such computed chemical shift difference is larger for **5** than for **6**, especially for the nonhelical structures, in agreement with the experimental spectrum of the first fraction, compared to that measured for the second fraction. For **6**, in addition, the NMR spectra computed for the two forms differ in that the chemical shift of the two H_b hydrogens is not equivalent for the nonhelical isomer. This computed result, in better agreement with the observed spectrum of the second fraction, showing a single but broader band for H_b, suggests a predominant nonhelicial structure for the second fraction. Accordingly, the first and second fractions can be assigned to the structures of **5** and **6**, respectively, an assignment which is further supported by comparison of the computed and experimental absorption spectra.

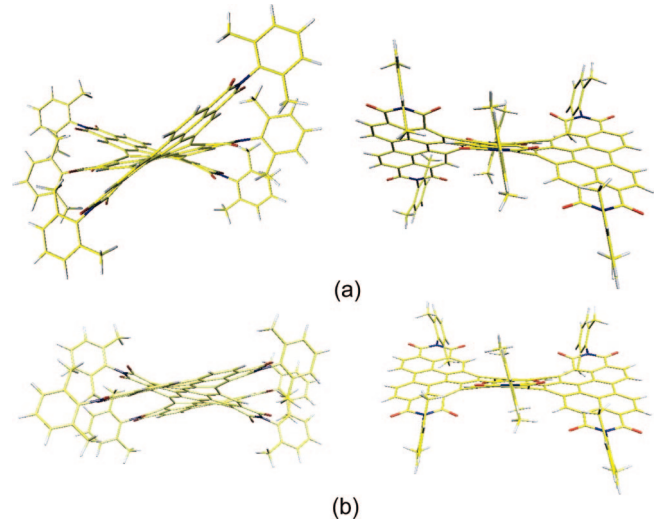

Figure 5. Helical (a) and nonhelical (b) structures of triPBI **5**.

Absorption Spectra. Compared to diPBI **4** (Figure S7, Supporting Information), triPBIs **5** and **6** (Figure 8) display

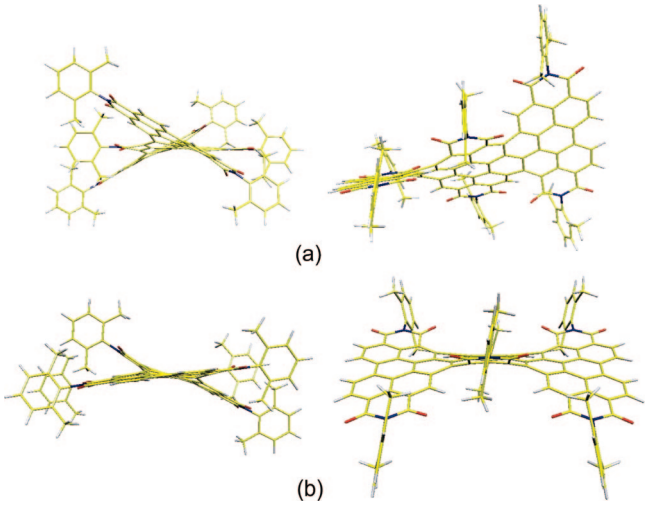

Figure 6. Helical (a) and nonhelical (b) structures of triPBI **6**.

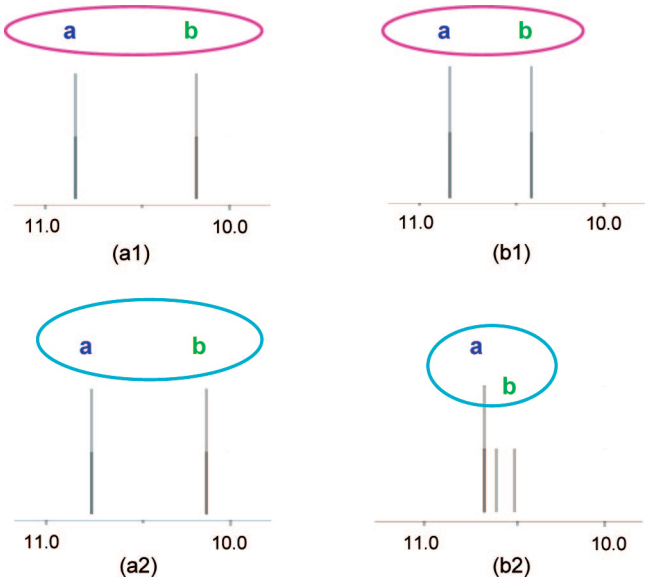

Figure 7. Portions of the B3LYP/3-21G computed ^{1}H spectra (chemical shift in ppm) of the helical (a) and nonhelical (b) configurations of **5** (1) and **6** (2).

broad and red-shifted spectra with major bands at 378, 426, 467, 508, 610, 681, and 750 nm and 372, 437, 508, 591, 700, and 805 nm, respectively. Examining the fully conjugated oligo-PBI series (PBIs to diPBIs to triPBIs), it is apparent that the energy of the lowest allowed electronic transition, namely the optical HOMO−LUMO gap, decreases and the number of absorption bands increases upon the addition of PBI units. The UV/vis spectrum of **6** is bathochromically shifted by about 55 nm with respect to that of **5**, suggesting a slightly more efficient conjugation in this as compared to triPBI **5**.

To confirm the assignment of structural isomers **5** and **6** and to assist the interpretation of the experimental absorption spectra, the absorption spectra were calculated for helical and nonhelical structures and are compared with the observed absorption spectra in Figure 8. The spectrum computed for the diPBI analogue of **5** and **6** is presented for comparison in the Supporting Information (Figure S7). It is seen that the TDDFT-calculated bands agree very well with the most prominent observed features in the experimental spectra, which further supports our assignment of **5** and **6** to the first and second fractions, respectively. The

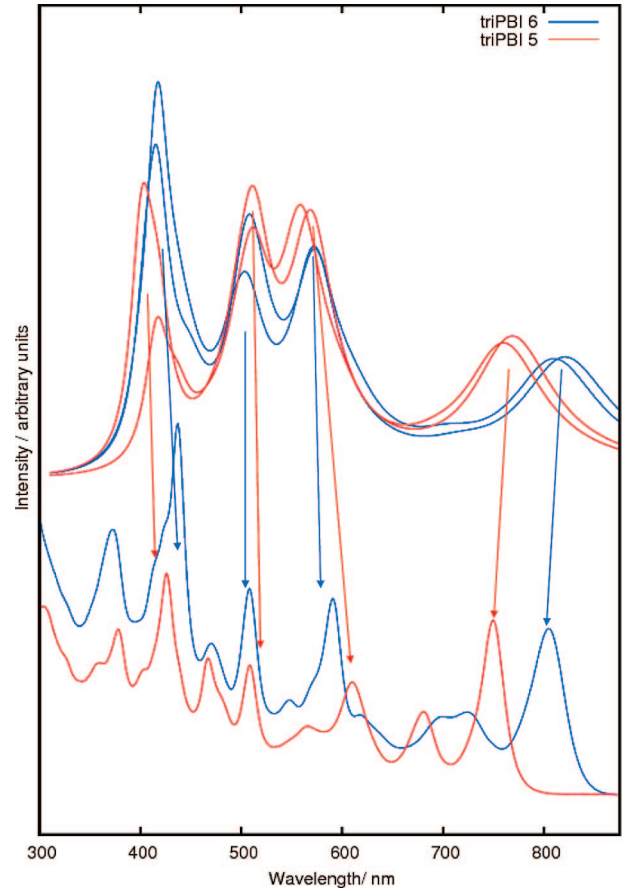

Figure 8. (Top) TDDFT-calculated absorption spectra of triPBI **5** (red) and triPBI **6** (blue). (Bottom) Absorption spectra of triPBI **5** (red) and triPBI **6** (blue) in $CHCl_3$.

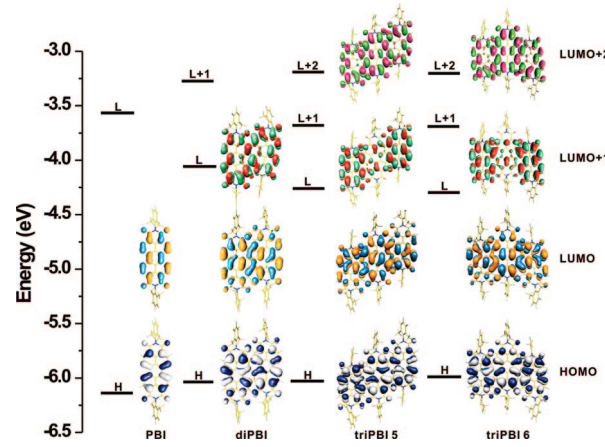

Figure 9. B3LYP/3-21G computed energies and shapes of the frontier orbitals of PBI, diPBI, and triPBIs at their equilibrium structures. The orbital shapes of the nonhelical structures of **5** and **6** are very similar to those of the helical species.

smaller number of bands in the computed spectra is due to the limited number of computed excitation energies and to the neglect of vibronic structures associated with the electronic transitions. Interestingly, it can be seen that the spectra simulated for the helical and nonhelical forms of each triPBI compound are very similar, and do not allow for discrimination between them. More importantly, the lowest energy excitation is predicted, invariably, for compound **6**, which may suggest a

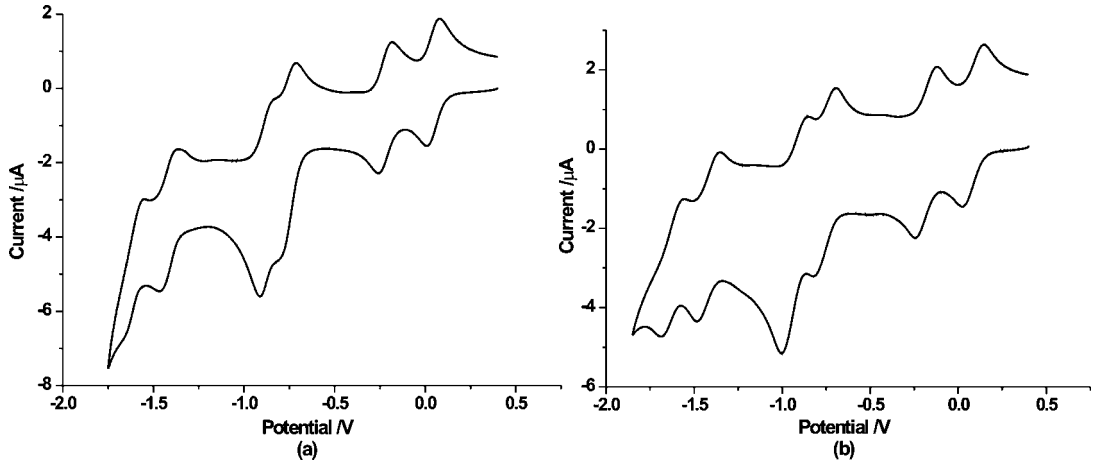

Figure 10. Reductive cyclic voltammograms of **5** (a) and **6** (b) in CH_2Cl_2. Scan rate, 0.1 V/s (electrolyte, 0.1 M $TBAPF_6$).

Table 1. Redox Potentials (in V vs Fc/Fc^+)[a]

	E_{1r}	E_{2r}	E_{3r}	E_{4r}	E_{5r}	E_{6r}
PBI **1**	−0.96	−1.22				
diPBI **4**	−0.46	−0.73	−1.49	−1.66		
triPBI **5**	−0.33	−0.60	−1.12	−1.26	−1.80	−2.00
triPBI **6**	−0.30	−0.57	−1.14	−1.30	−1.80	−1.99

[a] Half-wave potentials. The data have been recalculated to the reference of Fc/Fc^+. The oxidation potential of Fc/Fc^+ was measured as 0.40 V against Ag/AgCl.

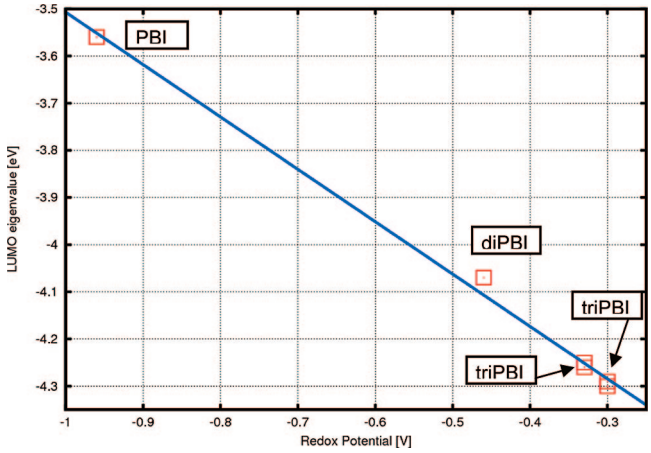

Figure 11. Computed LUMO energies (eV) versus the first reduction potentials (E_{1r} in V versus Fc/Fc^+) of PBI **1**, diPBI **4**, and triPBIs **5** and **6**.

slightly more efficient conjugation in this as compared to the parent triPBI **5**.

The optical gaps determined from absorption spectra are expected to reflect the trend in the HOMO−LUMO (transport) gaps since calculations show that the lowest allowed transition is dominated by the H→L single excitation. The shapes of the frontier orbitals of PBI and diPBI, and of the helical structures of triPBIs **5** and **6**, along with a schematic representation of their energy levels, are depicted in Figure 9, while energies and energy gaps are collected in the Supporting Information (Tables S1 and S2), together with the computed TDDFT excitation energies for the lowest allowed electronic transition.

The H−L energy gap follows the trend of the lowest energy transition upon the addition of PBI units, which is in agreement with the observed red-shifted absorption spectra. It should be noted, however, that the energy difference between the lowest energy transitions of **5** and **6** is small (0.11 eV), and the H−L gap is even smaller.

In the arrays of fully conjugated PBIs, the imide substituents have a negligible influence on the HOMO and LUMO orbitals because of the nodes at the imide nitrogens. As expected, the HOMOs of diPBI[20] and triPBIs[21] are linear combinations of the monomer's HOMO, and the lowest (two or three) unoccupied orbitals correspond to different linear combinations of the LUMO of PBI **1**. Calculations show that the energy of the LUMO lowers considerably when moving from PBI to diPBI to triPBIs. The computed trend suggests a concomitant increase of the electron affinity of these compounds. The increasing number of low-energy, unoccupied orbitals with similar parentage suggests an increasing ability to accept electrons, which is confirmed by the electrochemical properties discussed below.

Electrochemical Properties. The electrochemistry of fullerene derivatives exhibits six one-electron reduction waves, which is, to the best of our knowledge, the largest number for n-type organic materials.[22] According to the MO calculations, for diPBIs there are two unoccupied orbitals with the same parentage, the energies of which are very close. Thus, four electrons can be accommodated by diPBI, in agreement with the observed four reduction waves in electrochemistry.[12] Compared with diPBI, triPBIs have the lowest LUMOs and three unoccupied orbitals with the same parentage, implying their stronger electron affinity and the ability to accept up to six electrons. Cyclic voltammograms of triPBIs **5** and **6** display well-defined, single-electron reduction waves, two reversible, two quasireversible, and two irreversible (six in all, Figure 10). The half-wave reduction potentials vs Fc/Fc^+ of PBI **1**, diPBI **4**, triPBI **5**, and **6** are collected in Table 1. With the expansion of the π system by PBI units, the first reduction potentials of PBI arrays undergo a positive shift from −0.96 V for PBI **1** to −0.46 V for diPBI **4** to −0.33 V for triPBI **5**, and −0.30 V for triPBI **6**, indicating the increase in the electron-accepting ability. As revealed by the first reduction potentials, triPBI **6** is more

(20) Note that compared with the LUMO energy of PBI, for diPBI the LUMO energy is below, and that of the LUMO+1 is slightly above, as expected when making a linear combination of two orbitals.

(21) Notably, the LUMO+1 orbitals of triPBIs correspond to the combination of two LUMOs localized on external PBI units. The external units interact little, and hence the energy (−3.68 eV) of the corresponding orbital is very close to that of unperturbed PBI (−3.56 eV).

(22) (a) Xie, Q.; Pèrez-Cordero, E.; Echegoyen, L. *J. Am. Chem. Soc.* **1992**, *114*, 3978–3980. (b) Bendikov, M.; Wudl, Fred, *Chem. Rev.* **2004**, *104*, 4891–4945.

easily reduced than **5**, which is consistent with their calculated LUMO energies.

Accurate computational predictions of redox potentials require comparison of energies for both the starting molecule and its reduced forms. However, Koopmans's theorem[23] enables us to correlate the first redox potential of *x*PBI (*x* = mono, di, tri) systems with their LUMO energies. The result of such correlation is shown in Figure 11, where a plot of the computed LUMO energies versus the first reduction potentials shows good linearity. As shown in the plot, the change in LUMO energy and reduction potential from PBI to diPBI is quite big, while that observed from diPBI to triPBI is comparably smaller. The correlation suggests that, by adding new PBI units, the LUMO energy will lower further and the reduction potential will undergo a further positive shift, although both changes are expected to be small.

Conclusions

In summary, we report the copper-mediated trimerization of PBIs along bay regions to construct graphene nanoribbons that are functionalized by arrays of imide groups. Due to the two possible coupling positions, there are two structural isomers of triPBIs, **5** and **6**, which were successfully separated by HPLC. According to calculations, each of the two isomers has two possible conformers, corresponding to helical and nonhelical arrangements of the PBI units. The computed ^{1}H and absorption spectra for the two isomers of triPBIs agree very well with the observed spectra and allow the assignment of **5** and **6** to the first and second HPLC fraction, the computed NMR spectra suggesting also a predominance of the nonhelical isomer for compound **6**. With 19 benzene rings and 6 imide groups in the structures, triPBIs **5** and **6** display broad and red-shifted absorption spectra and six reduction waves in electrochemistry. Increasing the number of PBI units in oligo-PBIs (from PBIs to diPBIs to triPBIs) leads to an expansion of the π system, in turn associated with a reduction of the transport and optical band gaps (reflected in the UV spectra), the lowering of LUMO energies, mild reduction of the ionization potentials, and a remarkable increase in electron affinities, suggesting their potential applications as F-GNRs in organic electronics.

Acknowledgment. For financial support of this research, we thank the National Natural Science Foundation of China (Grant 50873106, 20421101), 973 Program (Grant 2006CB932101, 2006CB806200), and Chinese Academy of Sciences.

Supporting Information Available: Complete ref 17, experimental section, MS, ^{1}H and ^{13}C NMR spectra, DPV of **5** and **6**, optimized structures of **1** and **4**, comparison between computed and experimental absorption spectra of **4**, and tables with MO energies, absolute energies, and optical and transport gaps. This information is available free of charge via the Internet at http://pubs.acs.org.

JA807803J

(23) Koopmans, T. *Physica* **1934**, *1*, 104–113.